NASA Technical Memorandum 86964

Characterization of Lubricated Bearing Surfaces Operated Under High Loads

James L. Lauer and Norbert Marxer
Rensselaer Polytechnic Institute
Troy, New York

and

William R. Jones, Jr.
Lewis Research Center
Cleveland, Ohio

Prepared for the
International Tribology Conference
sponsored by the Japan Society of Lubrication Engineers
Tokyo, Japan, July 8-10, 1985

NASA

CHARACTERIZATION OF LUBRICATED BEARING SURFACES OPERATED UNDER HIGH LOADS*

James L. Lauer and Norbert Marxer
Rensselaer Polytechnic Institute
Troy, New York 12181
and

William R. Jones, Jr.
National Aeronautics and Space Administration
Lewis Research Center
Cleveland, Ohio 44135

SUMMARY

The composition and surface profiles of M-50 steel surfaces were measured after operation at high loads in a bearing contact simulator. An ester lubricant (trimethyolpropane triheptanoate) was used with and without various additives. Optical profiles were obtained to ±30 Å depth resolution with a phase-locked interference microscope in 10 μm diameter areas within and outside the wear tracks. Optical constants and surface film thickness were measured in the same areas with an electronic scanning ellipsometer. Film composition was measured with a scanning Auger electron spectrometer. It was concluded that metal oxide formation was accelerated within the wear tracks.

E-2462

INTRODUCTION

Lubrication has been recognized as a surface phenomenon for a long time and is of enormous importance in modern civilian and military technology. Nevertheless, the changes occurring on a microscale, which must precede macroscopic changes, such as failures by scuffing, are still mostly unknown. Obviously, the understanding of these changes offer much promise toward solving these bearing problems.

Many new methods of surface analysis have been developed in recent years (refs. 1 and 2). However, since these methods often require the use of high vacuum and electron bombardment, they may be destructive to the surface being analyzed. Furthermore, these techniques normally furnish only elemental information and their spatial resolution is not high.

Recently, we have had access to a scanning Auger spectrometer (AES); its best spatial resolution of about 50 μm is very good. However, most of our work (refs. 3 and 4) has utilized a phase-locked interference microscope (PLIM) having a spatial resolution of better than 20 μm and an electronic scanning ellipsometer (ESE). These were used to measure surface changes of a simulated bearing contact operated on its way to failure.

---

*This work was sponsored by NASA Lewis Research Center Grant NAG 3-222. Additional funding was provided by Air Force Office of Scientific Research Grant AFOSR-81-0005 and by Army Research Office Grant DAAG 2483K0058.

Significant changes were found, (1) in surface profiles within the wear track during bearing operation for different lubricants, (2) in the rate of oxidation of the bearing surfaces within and outside the wear track, (3) in the rate of change of optical profile within and outside the wear track after brief exposure to dilute hydrochloric acid, and (4) in the friction for different lubricant formulations (refs. 3 and 4).

The objective of this paper is to summarize the surface analytical results obtained from a simulated bearing contact. Three instruments were used: (1) a phase-locked interference microscope, (2) an electronic scanning ellipsometer, and (3) a scanning Auger spectrometer. Materials used included an M-50 steel ball and plate and lubricants (trimethyolpropane triheptanoate) simulating MIL-L-23699 and its additives.

MATERIALS

The lubricants were trimethylolpropane triheptanoate either alone or with one or all of the following additives, (1) benzotriazole (0.0203 wt %, corrosion inhibitor, BTZ), (2) dioctyl-diphenylamine, (3) phenyl-α-napthylamine (both 1.036 wt %, antioxidants, DODPA and PANA), and (4) tricresylphosphate (2.55 wt %, antiwear additive, TCP). The fully formulated lubricant is equivalent to MIL-L-23699 and is designated as G-MIL-99. Properties of the base fluid appear in table I.

The probe solution was 0.04 M hydrochloric acid in ethanol. The ball and plate were hardened martensitic M-50 steel (Rockwell C, 62-63) (0.8 percent C, 41.1 percent Cr, 1.0 percent V, 4.25 percent Mo).

APPARATUS AND PROCEDURE

Bearing Contact Simulator

A schematic of the bearing contact simulator appears in figure 1. The simulator consists of a M-50 steel bearing ball (20.6 mm diam) supported by two bearings and driven by an electric motor through a horizontal shaft. The ball is loaded from the top by a M-50 plate supported by linear bearings on a horizontal loading platform. The friction force is measured by the strain generated in a leaf spring connecting the plate with the loading platform. Lubricants were injected into the contact from a reservoir at ambient temperature by a peristaltic pump.

The maximum Hertzian pressure was 0.1 GPa. Ball speed was 220 rpm (0.2 m/s surface speed). Test duration was 30 min at which time the friction force had reached a steady value.

No attempt was made to control or measure contact temperature. However, an estimate of the maximum surface temperature based on Winer's results (ref. 5) indicate that the temperature may exceed 220 °C. This is in excess of the critical temperature for TCP surface reaction according to Faut and Wheeler (ref. 6).

Phase-Locked Interference Microscope (PLIM)

This instrument, schematically shown in figure 2, is basically a Michelson interferometer with a laser source and microscope objectives facing two mirrors at almost equal distances from the beamsplitter. One of these mirrors is the reference mirror which is vibrated piezoelectrically at 20 kHz. The other "mirror" is the sample surface, which can be translated horizontally to bring surface features of different heights into the field of view. Reflected radiations from these mirrors are recombined at the beamsplitter and passed through another microscope objective to bring enlarged interference fringes onto a photodetector. If the two beamsplitter-to-mirror distances are equal the photodetector is "locked" into the peak of a fringe and the 20 kHz amplitude vanishes. If they are not equal, an error signal is generated, resulting in a dc potential on the piezoelectric crystal to shift its plane in such a way as to make the distances equal. A plot of dc potential against the horizontal sample position results in the "optical" profile of a surface. It is the optical profile rather than the true physical profile because in reality phases and not distances are compared and phases depend on the optical constants of the surface layer and its thickness as well as on the optical properties of the substrate. For this reason the profiles obtained with different laser wavelengths are different when different surface layers, e.g., oxides on steel, are present. From these differences the nature and thickness of the oxides can be deduced provided some of the optical constants are independently known, e.g., ellipsometrically.

Electronic Scanning Ellipsometer (ESE)

A schematic diagram of the ellipsometer is shown in figure 3. This is the ellipsometer originally designed by Monin and Boutry (ref. 7), which was modified by Sullo and Moore at the University of Rochester (ref. 8). Radiation from the laser source S is polarized by the polarizer P, whose azimuth of vibration with respect to the plane of incidence in θ. On reflection from the sample surface M, the plane-polarized radiation has become elliptically polarized. The angle of the semi-major axis of the ellipse and the plane of incidence is γ. CF is a Faraday modulator consisting of a solenoidal coil with a Faraday glass cylinder at its axis. The magnetic field generated by the coil causes the azimuth of polarized radiation of the light traveling along the axis of the cylinder to be changed proportionally to the magnitude of the magnetic field and to the length of the cylinder, the proportionality constant being called the Verdet constant. This phenomenon is known as the Faraday effect. The coil is driven by a 500 Hz oscillator, causing the magnetic field to vary with that frequency. By the Faraday effect, the inclination angle of the polarization ellipse with respect to the plane of incidence is also varied with the same frequency. The radiation from the Faraday modulator is passed through the polarization analyzer A of the azimuth β and is finally detected by the photocell or photomultiplier PM.

Our instrument uses a 10 cm long, 0.6 cm diameter Faraday glass cylinder (three times as long as Sullo's) in order to obtain a large amplitude of modulation. The current in the coil is modulated with a 500 Hz frequency. If the analyzer angle β is equal to the true azimuth γ, the radiation detected at the 500 Hz frequency by phase-sensitive electronic detector is zero and the electronic system is "locked." At the same time, the amplitude of the first harmonic (100 Hz) is monitored to make sure it is nonzero. If, however, the

amplitude detected at 500 Hz is nonzero, an error signal is used to turn the analyzer by an angle appropriate to make it zero. This is done by an electro-optic transducer and control circuit capable of resolving 0.01° of arc.

Scanning of a sample surface is done by moving the sample M parallel to its plane while the polarizer is rotated at an essentially constant speed with a dc motor and the analyzer is being continuously reset at corresponding azimuths. Plots of polarizer versus analyzer angle look like the curve of figure 4. One method of obtaining the ellipsometric parameters ψ and Δ from this curve is graphically as shown in the figure. However, our computerized curve fitting program is much more accurate, because all the data points on the curve as used, not just a few selected ones. Furthermore, many such curves can be traced and averaged in a short time. Once Δ and ψ are known, the index of refraction n and the film thickness can be calculated, but since n is complex, consisting of two variables, more than two measurements are needed, e.g., at more angles of incidence (not just at 45°), different wavelengths, etc. The computations can become quite extensive, but are easily performed on a small laboratory computer.

By placing a microscope objective forming a real image of the sample surface ahead of the detector, sample areas as small as 20 μm in diameter can be resolved ellipsometrically. Most of the energy reflected of the surface is lost, but sufficient energy remains to make the measurements.

RESULTS

Friction and Surface Roughness

Effect of the acid probe. - Figure 5 shows friction versus time curves for the different lubricant formulations after the ball and plate had been soaked in them for 3 hr at ambient temperature.

The operating conditions were such that scoring or scuffing would occur very soon for the fully formulated oil, thereby allowing us to maximize the differences for the additives. Differences between the bearing surfaces for the antioxidants and TCP with and without soaking were found. The surface roughnesses (standard CLA roughness) were determined from the optical profiles and plotted in figure 6. The antioxidants DODPA and PANA show the least change over the measured time period within the error limits. DODPA and PANA are also the only additives giving a significant reduction of roughness in the initial phase of operation when the acid probe was applied. Since these measurements were made in separate experiments, the consistency of the friction, roughness, and acid probe data must be significant. Another interesting observation is the sharp increase in relative roughness change after acid treatment for both BTZ and TCP in the final stage of the test, while the roughness change remained about constant during most of the run.

A closer examination of figure 6 reveals some interesting correlations. Since the vertical scale is arbitrary and the curves were displaced by arbitrary amounts to avoid confusion, only trends are significant. The fully formulated oil (G-MIL-99) and the two amine additives PANA and DODPA gave rise to roughness peaks at about 20 sec. The fully formulated oil, the base oil and BTZ, the anticorrosion additive, had roughness peaks at about 80 sec. Only TCP

shows a descending slope beyond 100 sec. These differences might be related to the formation of different surface oxides.

The two surface additives TCP and BTZ had the highest friction while the antioxidants had the lowest. All the surfaces were soaked for 3 hr in the respective lubricants, cleaned and dried, and then immediately used in the friction test with clean base oil.

Ellipsometry of Wear Tracks

In figure 7, the changes of slope, cos Δ/tan ψ, were plotted across the wear track for the samples of figure 5. It will be noted that TCP, which had the highest friction in figure 5, also shows the greatest variation over the traverse. The sharp positive and negative peaks correspond to a spot on the wear track (between 100 and 500 μm on the abscissa), which is clearly visible under the microscope. The half-widths of these peaks is about 20 μm. The slope changes for the other materials inside the wear track were much smaller. Outside the wear track the slope variations were minimal; the bottom curve for DODPA shows the characteristic behavior there. Clearly, the nature of the surface is different inside the wear track. The change is not caused by a change of reflecting angle for the reflected laser beam is very restricted by apertures. When the angles and corresponding azimuths were changed in order to compute the film thickness and the optical constants, the former came out to be about 60 Å at the maximum and the latter correspond roughly to Fe_2O_3 by comparison with the data of Leberknight and Lustman (ref. 9). The identification is tentative and not unique for lack of reference data, which will be obtained later. The preferential production of a thin oxide layer on wear tracks would seem to be general, but is strongest for those produced in the presence of TCP.

It should be pointed out that the collection of data such as those of figure 7 presents problems different from those encountered when ellipsometry is used with dielectric substrates (ref. 10). Most ellipsometric work today refers to dielectrics and semiconductors. The most important difference is reflectivity - high for metals and low for dielectrics and semiconductors. Furthermore, metals have a complex index of refraction (two optical constants), dielectrics only a real index of refraction.

Auger Electron Spectroscopy

The plates were analyzed after experiments with each additive. Three areas were selected, two within the wear track and one outside of it for reference. After the experiment, the specimens were washed with alcohol and allowed to dry prior to their introduction into the Auger spectrometer. As a control, a polished M-50 plate not used in an experiment was included in the set of Auger analyses.

All the lubricant formulations and the reference gave about the same initial spectra. However, after 6 min of ion bombardment, all the spectra from outside the wear scar as well as from the reference plate were essentially free of O and C. Those from inside the wear scar, notably those from TCP and from BTZ had a higher O and C content.

In order to show the effect of ion bombardment on elemental composition, the plots of figure 8 were drawn for two positions within the wear scar. They present the ratios of the O and C peaks to one of the Fe peaks as a function of time. A sharp change of slope after 2 to 4 min probably signifies the removal of a surface layer.

From these observations, the following deductions can be made:

(1) The high C-ratios and O-ratios in the outermost surface layer are probably atmospheric contamination. They are present even in the reference.

(2) TCP has an oxide layer under the atmospheric contamination layer. BTZ is likely to have one as well. The reference, however, does not have such a layer within our error of measurement, but the other materials might have a weak oxide layer.

(3) A carbide layer might also underly the atmospheric contamination layer.

DISCUSSION AND CONCLUSION

In our previous publications (refs. 3 and 4) the difference in the effect of dilute hydrochloric acid (our acid probe) on causing contour changes within and outside a wear track was described. This difference was especially great when scuffing conditions were approached. It was also found that the presence of the antiwear additive TCP in the lubricant would enhance this difference. Then the question was raised why scuffing could occur so suddenly, apparently without warning, even though operating conditions could have been far from those postulated by the Blok temperature criterion. A principal objective of this study was to try to explain the behavior of the acid probe in the hope that an answer would also help in arriving at an answer to the latter question.

Differences in the optical profile at different wavelengths, ellipsometry; and Auger electron spectroscopy have now been shown to discriminate between the surface within the wear crack on M-50 steel and outside of it. The evidence points to a higher concentration of an oxide, most likely iron oxide, within the wear track. Interestingly enough, it would seem that TCP promotes the formation of such an oxide. Such an oxide would react much faster chemically with acid than the alloy steel itself. Thus, the oxide would explain the behavior of the hydrochloric acid probe. The oxide is more likely to be formed in the wear track than outside of it because of the higher surface temperature in the wear track. It would also reduce friction at higher temperatures, though not at low ones and explain both our data of figure 5 and the results of Faut and Wheeler (ref. 6). Although such an iron oxide layer on the surface could conceivably promote the formation of friction polymer-whose formation was reported to be enhanced by TCP also-it is more likely that the same oxidizing conditions that lead to the formation of the oxide also lead to the formation of friction polymer. Friction polymer is, in turn, related to acid sludge. The acid is likely to react quickly with the basic iron oxide provided the temperature is high enough. Therefore a case could be made for a mechanism of scuffing. This is, removal of the oxide layer by reaction with acids in the lubricant exposes the nascent metal and allows metal-to-metal welds. Work now in progress in our laboratory will test this idea.

A new metallurgical phase for M-50 steel was also found and reported in our earlier publication (ref. 4). Its etching characteristics seemed to identify it as a carbide. The higher carbon contents found in the wear track below the surface, especially for TCP, are consistent with this identification.

The sharp initial decrease in the experiment of acid probe reactivity of the two amine antioxidants can be explained by the initial formation of an amine surface film and subsequent exposure of the original alloy steel surface, i.e., the lack of a surface oxide. Since the metal reacts more slowly than the oxide-which was prevented from forming-the probe reaction slows down. Once the amine antioxidant is exhausted, the reaction speeds up again, however, thus explaining the increased activity later. The amine surface film could also be instrumental in reducing friction.

The behavior of BTZ, the anticorrosion additive, has been found to be similar to TCP in some ways. Its low oil solubility requires its small concentration. By the same token, it is more likely to come out of solution and coat the bearing surfaces with an anodic (ref. 11) layer. However, as Parkins (ref. 11) admits, the behavior of these materials is still not well understood, even by electrochemists, though they have been used for a long time.

Thus, it would seem that leads have been generated to help in the design of lubricating materials to reduce friction and scuffing failures. Their chemical interaction with the bearing surfaces, i.e., the formation of oxide and perhaps other layers is an important key.

REFERENCES

1. Ferrante, J., "Practical Applications of Surface Analytic Tools in Tribology," Lubr. Engr., 38, pp. 223-236 (1982).

2. Kane, P.F. and Larrabee, G.B., "Characterization of Solid Surfaces," Plenum Press, New York, 1974.

3. Lauer, J.L., and Fung, S.S., "Microscopic Contour Changes of Tribological Surfaces by Chemical and Mechanical Action," ASLE Trans., 26, pp. 430-436 (1983).

4. Lauer, J.L., Fung, S.S., and Jones, W.R., Jr., "Topological Reaction Rate Measurements Related to Scuffing," ASLE Trans., 27, pp. 288-294 (1984).

5. Ausherman, V.K., Nagaraj, H.S., Sanborn, D.M., and Winer, W.O., "Infrared Temperature Mapping in Elastohydrodynamic Lubrication," J. Lubr. Technol., 98, p. 236-243 (1976).

6. Faut, O.D., and Wheeler, D.R., "On the Mechanism of Lubrication by Tricresylphosphate (TCP) - The Coefficient of Friction as a Function of Temperature for TCP on M-50 Steel," ASLE Trans., 26, pp. 344-350 (1983).

7. Monin, J., and Boutry, G.A., "Principle, Realization and Performance of a New Ellipsometer," Nouv. Rev. Opt. Appl., 4, pp. 159-169 (1973).

8. Sullo, N.J., "Measurement of Absolute Refractive Index Profiles in Gradient Index Materials Using Modulation Ellipsometry." M.S. Thesis, University of Rochester, 1982.

9. Leberknight, C.E., and Lustman, B., "An Optical Investigation of Oxide Films on Metals," J. Opt. Soc. Am., 29, pp. 59-66 (1939).

10. Vedam, K., "Characterization of Surfaces," The Characterization of Materials in Research: Ceramics and Polymers, ed. by J.J. Burke and V. Weiss, Syracuse University Press (1975) pp. 503-537.

11. Parkins, R.N., "Corrosion Inhibition," Comprehensive Treatise of Electrochemistry, Vol. 4; Electrochemical Materials Science, ed. by J. O'M Bockris, B.E. Conway, E. Yeager, and R.E. White, Plenum Press, New York (1981) pp. 313-315.

TABLE I. - PROPERTIES OF TEST FLUID (TRIMETHYOLPROPANE TRIHEPTANOATE)

Kinematic viscosity, m^2/sec (cS)	
At 98.9 °C	3.5×10^{-6} (3.5)
At 37.8 °C	1.52×10^{-5} (15.2)
At -17.8 °C	2.87×10^{-4} (287)
At -40 °C	2.4×10^{-3} (2400)
Pour point, °C	-68
Specific gravity, 25 °C	0.963
Moisture content, percent	0.02

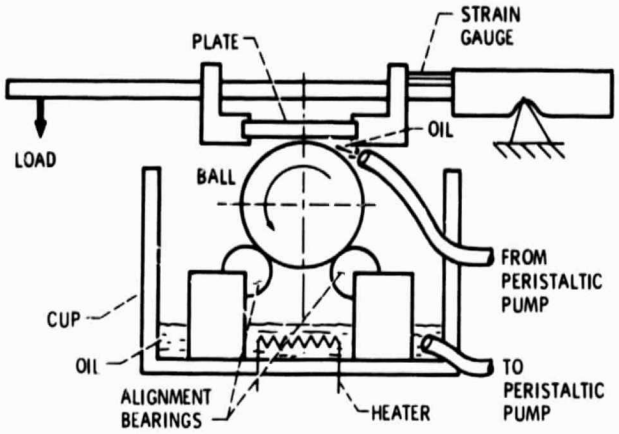

Figure 1. - Schematic of bearing contact simulator.

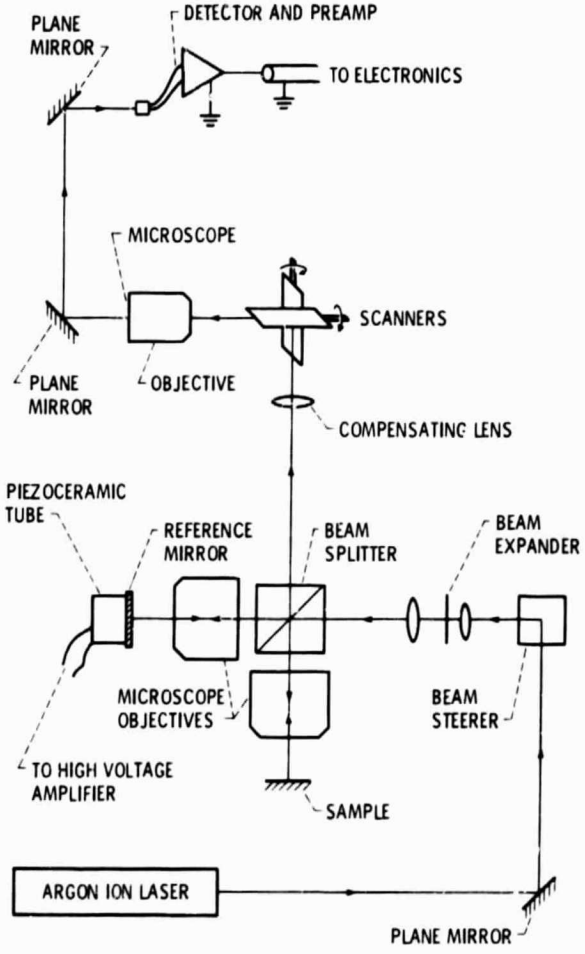

Figure 2. - Schematic drawing of phase-locked interference microscope (PLIM).

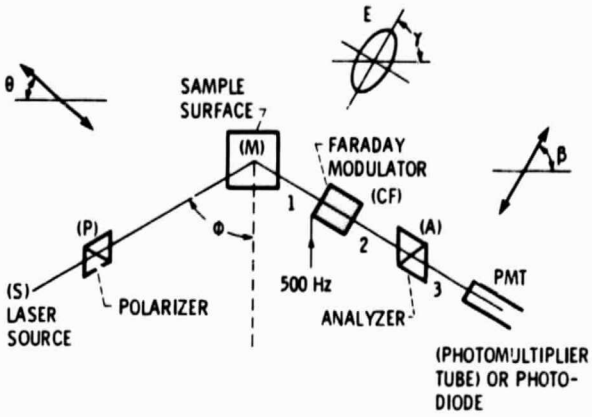

Figure 3. - Schematic drawing of electronic scanning ellipsometer (ESE).

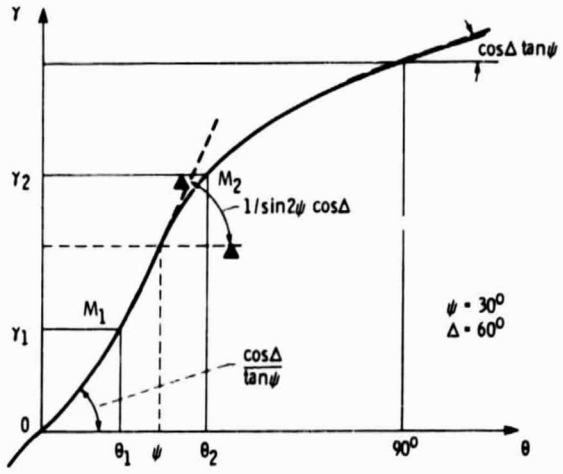

Figure 4 - Determination of the ellipsometer parameters.

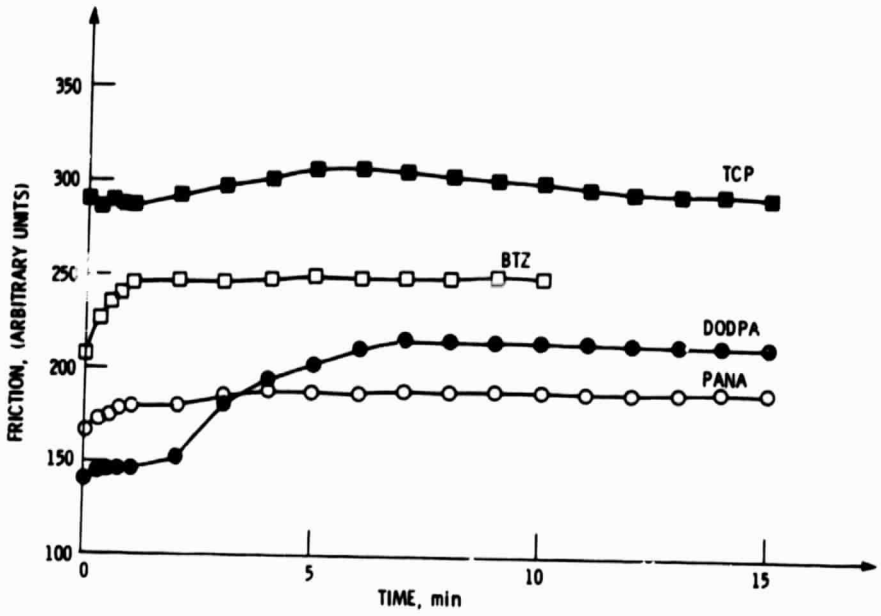

Figure 5. - Friction as a function of time for various lubricant formulations.

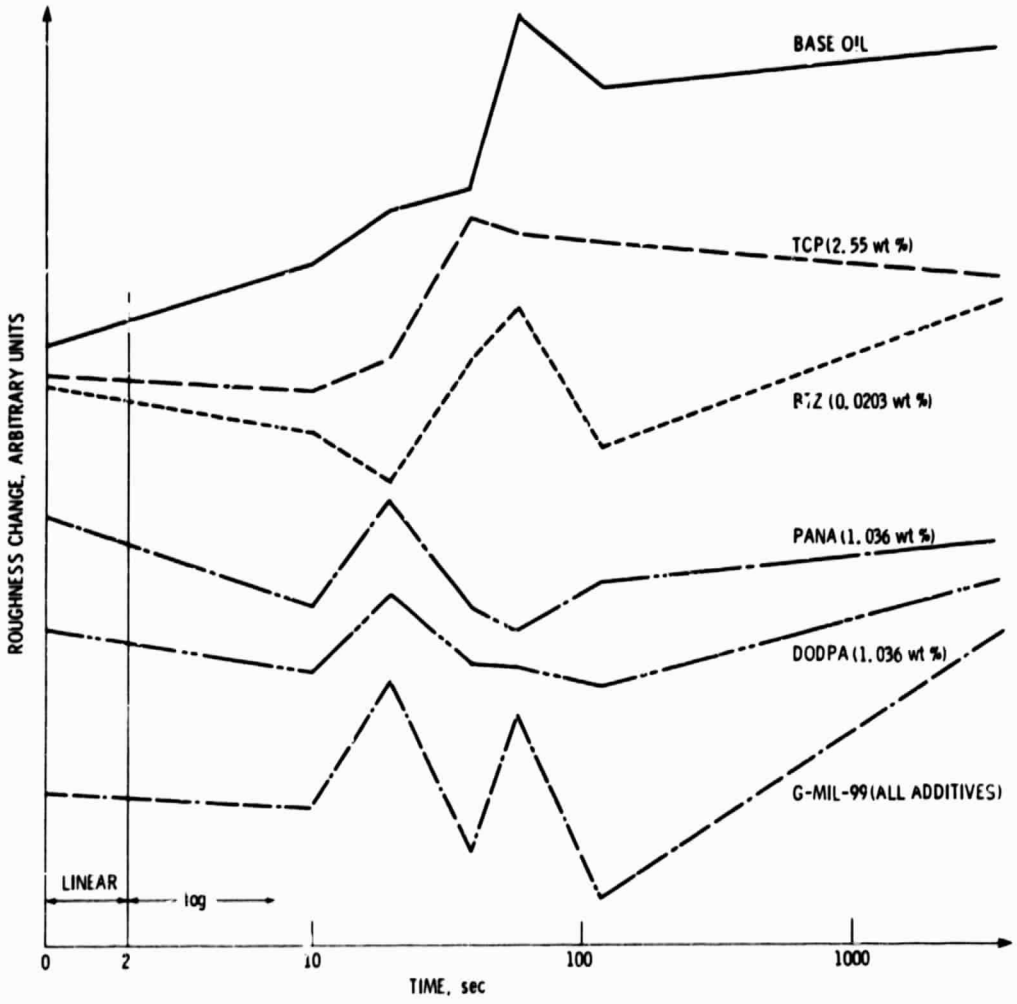

Figure 6. - Roughness changes with operating time of bearing contact. The units of the ordinate are arbitrary, but equal for all the lubricants. The curves for the different lubricants are displaced vertically to reduce confusion. Roughness is defined as the area on the optical profile plot, which is bounded by the center line and the curves above and below for an arbitrary distance.

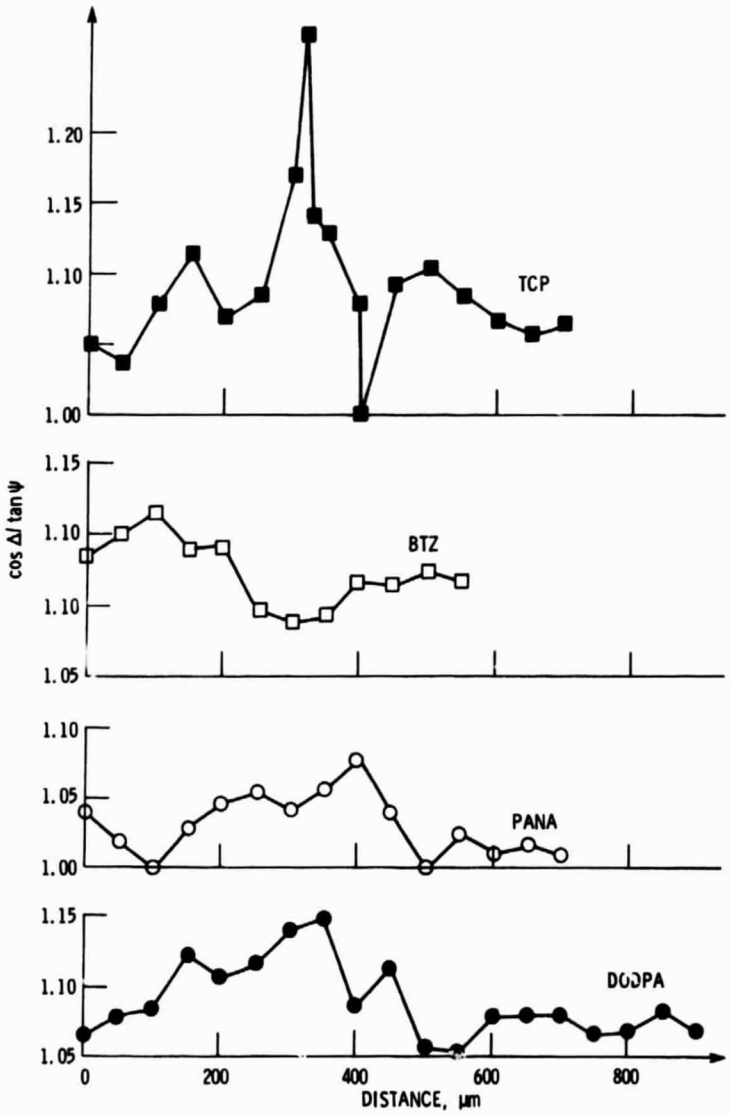

Figure 7. - Ellipsometric slopes from wear tracks using different lubricant formulations.

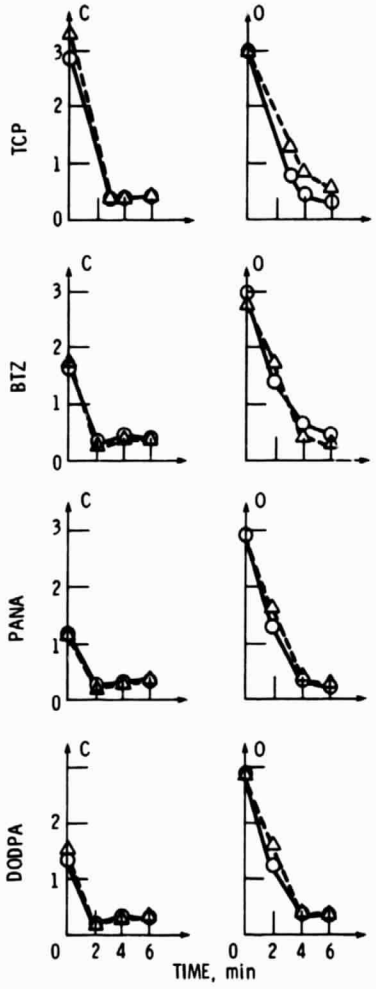

Figure 8. - Ratio of a carbon to an iron Auger peak (left) and of an oxygen to the same iron peak (right) for ion bombardment times of zero to six min (10Å are removed per minute). The solid and broken lines refer to two different spots within the wear track.